OBSERVATIONS OF SUPERNOVA REMNANTS

A. Decourchelle
Service d'Astrophysique, DAPNIA, DSM
CEA Saclay, L'Orme des Merisiers
F-91191 Gif-sur-Yvette, France
ADECOURCHELLE@CEA.FR

Abstract

Shocks in supernova remnants are long thought to be responsible for the acceleration of Galactic cosmic rays up to the knee (above 1000 TeV). Synchrotron radio emission attests to the presence of GeV accelerated electrons. With the advent of X-ray spectro-imagery, observational evidence has been obtained for the acceleration of electrons up to energies of about 100 TeV. I will review the recent observations of non-thermal emission in young ejecta-dominated supernova remnants and in synchrotron-dominated supernova remnants like SN1006 and G347.3−0.5. I will illustrate the importance of combining X-ray and radio data for characterizing the synchrotron emission and its spectral variations, as well as for studying the interaction of the blast wave with the ambient medium. These results are crucial for the understanding of particle acceleration in supernova remnants and the origin of the Galactic cosmic rays. They uniquely provide constraints on poorly known aspects of particle acceleration like the magnetic turbulence, the acceleration efficiency and, potentially, the level of particle injection.

1 Introduction

In young supernova remnants (SNRs), the main physical process is the interaction of high velocity ejecta with the ambient medium, which gives rise to two shocks. While the forward shock is propagating outward in the ambient medium, the reverse shock (which is associated to the deceleration of the ejecta by the non negligible pressure of the shocked ambient medium) is propagating inward in the ejecta. This interaction region, bounded by these two shocks, is heated to temperature of tens of million degrees and emits copious X-ray thermal bremsstrahlung and line emission. In this phase, the shocked ejecta dominate the overall X-ray emission due to their larger density, lower temperature and enhanced heavy elements abundances, producing strong K-lines of mainly Si, S and Fe as is observed in the young remnants of Cas A (Hughes et al., 2000; Hwang et al., 2000), Tycho (Decourchelle et al., 2001; Hwang et al., 2002) and Kepler (Cassam-Chenaï et al., 2004a).

Both the composition of the ejecta and the spatial distribution of the elements are crucial information for constraining the supernova progenitor, deriving the nucleosynthesis products, the level of element mixing and the development of Rayleigh-Taylor instabilities.

At later stage, when the mass swept up by the forward shock is larger than the ejected supernova mass, the ejecta contribution becomes negligible. The evolution of the SNR depends then mainly on the structure of the ambient medium (stellar wind, wind-blown bubble, interstellar clouds), in which the forward shock is propagating. Both radio and X-ray observations are crucial to understand this phase. In particular, when the remnant is interacting with interstellar structures (clouds, shell), radio thermal H I and CO line emission can provide the distribution of interstellar clouds and reveal shock interaction with clouds via maser emission.

The shock waves not only compress and heat the swept-up material, but also can accelerate particles via first order Fermi acceleration (see Kirk, 2005; Reynolds, 2005) as testified by synchrotron radio observations, which reveal the presence of relativistic ($\simeq$ GeV) electrons at the forward shock. For a long time, SNRs have been considered the best source of cosmic rays with energy up to the knee: they have strong shocks where first-order Fermi acceleration can proceed, the index of their synchrotron spectrum is close to theoretical expectation, and with 10% of their explosion energy in the acceleration process, they can ac-

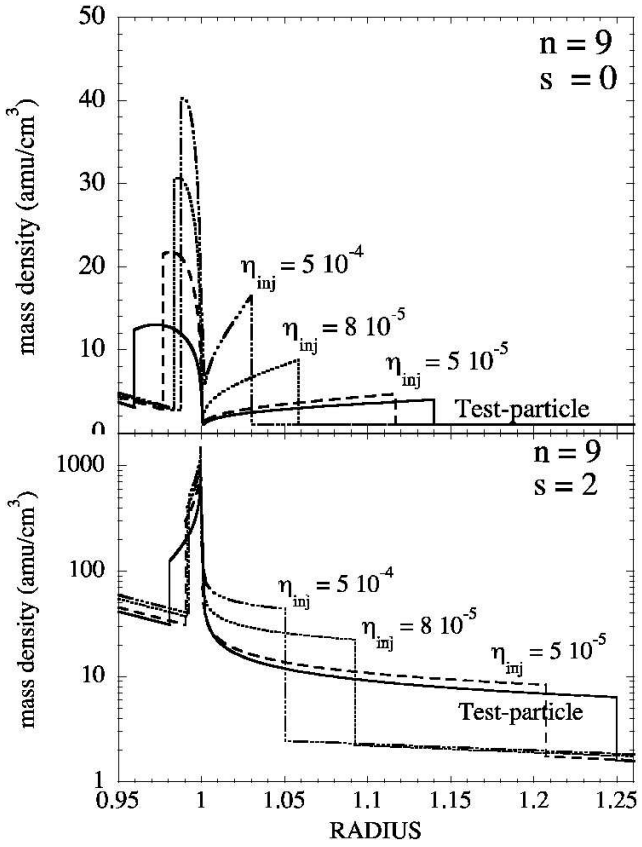

Figure 1: Density profile versus radius for the interaction region for different values of the injection parameter $\eta_{\rm inj}$. For the ambient medium, we have considered two cases: a uniform interstellar medium (top) and a stellar wind (bottom). In both cases, the initial ejecta density profile is a power law of index n = 9. The upstream magnetic field value is 3 μG, assumed to be the same at the forward and reverse shocks.

count for the pool of galactic cosmic rays.

The advent of CCD X-ray spectro-imagers has allowed to obtain the first evidence of electrons accelerated up to TeV energies in the remnant of SN1006 (Koyama et al., 1995). The bright X-ray and radio limbs were revealed by the *ASCA* satellite to be spectrally featureless and interpreted as X-ray synchrotron emission from TeV electrons, while in the faint areas (center and faint limbs) the emission was thermal. To further confirm this interpretation, TeV emission of the brightest limb of SN1006 was observed from the CANGAROO ground based Cherenkov detector (Tanimori et al., 1998). This result, as well as the subsequent discovery of two other synchrotron dominated SNRs, G347.3−0.5 (or RX J1713.7−3946, Koyama et al., 1997; Slane et al., 1999) and G266.2−1.2 (or RX J0852.0−4622, Slane et al., 2001), have shown the potential of X-ray observations to observe the highest energy electrons that shocks in SNRs can accelerate. However, a characterization of the synchrotron emission and of its variation over the remnant had to wait for the current generation of X-ray satellites (*Chandra* and *XMM-Newton*) to combine reasonably good spectral and spatial resolution. Such characterization of the synchrotron spectrum requires both radio and X-ray data.

In this review, I will thus focus on the search for observational constraints on particle acceleration in SNRs, for which radio and X-ray data are necessary. Although much progress has been made over the last ten years there are still several pending questions in regards to 1) the efficiency of cosmic ray acceleration in SNRs, 2) the maximum energy particles can reach at their shocks, 3) the strength (is it amplified?) and orientation (ordered or turbulent) of the magnetic field, and 4) the evidence for ion acceleration in SNRs. Section 2 is dedicated to the search of observational constraints on the efficiency of particle acceleration at the forward shock in SNRs based on their morphology and X-ray spectroscopy. Section 3 will focus on the efficiency of particle acceleration at the reverse shock. Finally in the last section, I will discuss the geometry of the acceleration in SN1006 and the spatially resolved spectral characterization of the synchrotron emission in G347.3−0.5.

2 Search for efficient particle acceleration in young supernova remnants

When particle acceleration is efficient (non negligible amount of energy in the acceleration process), nonlinear effects cannot be ignored (Drury, 1983, 2001). The feedback of the accelerated particles (protons and heavier elements) modifies the shock structure, leading to compression ratios which can be much larger than the value of four expected for strong shocks, and hence to post-shock temperatures lower than expected in the non modified test-particle case. The shock compression ratio increases with the fraction of particle injected and strongly impacts the morphology of the interaction region, which gets much narrower as the number of injected particle increases (see Fig. 1).

We use the framework of self-similar hydrodynamical models (Chevalier, 1982, 1983; Decourchelle et al., 2000) to show the impact of particle acceleration on

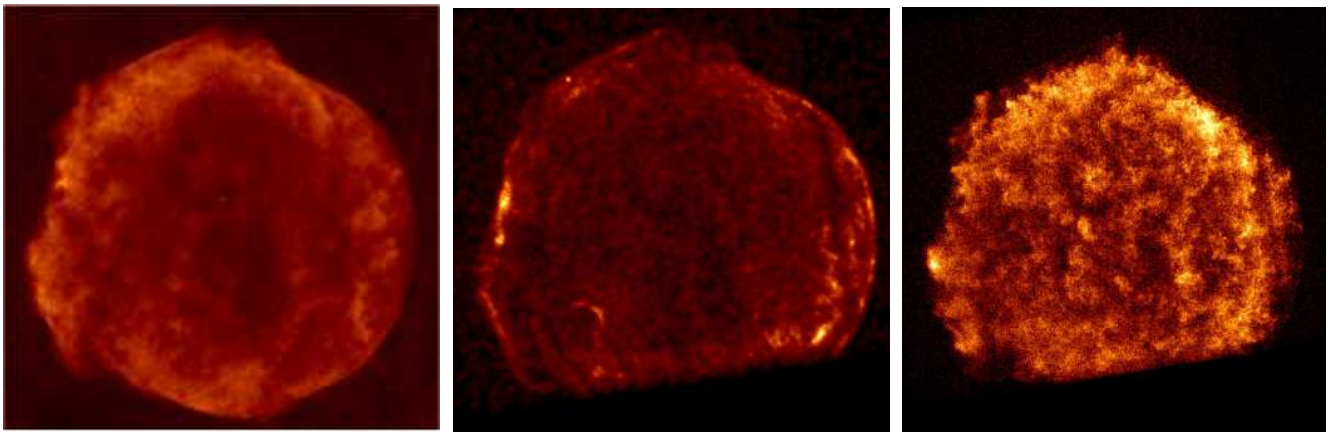

Figure 2: Images of Tycho's SNR (SN1572) in the radio (left), in the 4–6 keV X-ray continuum (middle) and in the silicon heliumoïd K-lines (right). The X-ray images have been obtained with *Chandra* satellite, see Hwang et al. (2002).

the morphology of the interaction region. We assumed an initial ejecta density power law profile of index n = 9 and considered two different cases for the ambient medium of density $\rho \propto r^{-s}$: a uniform interstellar medium (s = 0) and a stellar wind (s = 2). For the sake of simplicity, the upstream magnetic field is considered to be the same at the reverse shock and at the forward shock, which is not necessarily the case as is discussed in Sect. 3. Figure 1 shows the density profile versus radius of the interaction region for different values of the injection parameter $\eta_{\rm inj}$ (see Berezhko & Ellison, 1999, for a definition of this parameter). The case of a uniform interstellar medium is shown in the top panel, while that of a stellar wind is shown in the bottom panel. These density profiles differ strongly depending on the nature on the ambient medium as already discussed by Chevalier (1982). The main morphological effect of efficient particle acceleration is to shrink the interaction region. As a result, the forward shock is much closer to the contact discontinuity than in the unmodified test-particle case (Decourchelle et al., 2000; Ellison et al., 2004). In particular, for a uniform interstellar ambient medium, the separation between the interface and the forward shock becomes very small. In the test-particle case, the forward shock was already twice as close as for s = 2. This separation depends also on the index n of the initial ejecta density profile (Chevalier, 1982): the smaller the index, the larger the separation.

Two dimensional hydrodynamical simulations of the SNR evolution have been carried out with different values of the effective adiabatic index ($5/3 \leq \gamma \leq 1.1$) to mimic the effect of efficient particle acceleration on the interaction region (Blondin & Ellison, 2001). This modifies slightly the development of Rayleigh-Taylor instabilities at the contact discontinuity (between the ejecta and the ambient material). The most noticeable effect is that the Rayleigh-Taylor fingers can now reach and perturb the forward shock. This is due to the much closer proximity of the forward shock than in the test-particle case and can be considered as a signature of efficient particle acceleration. Attempts to reproduce such perturbation of the forward shock due to Rayleigh-Taylor fingers were previously unsuccessful (Chevalier & Blondin, 1995) unless the supernova remnant expands into a clumpy circumstellar medium (Jun, Jones & Norman, 1996). Based on these predictions, I will examine the radio and X-ray morphology of several young ejecta-dominated SNRs.

2.1 Radio and X-ray morphology of the interaction region

The Very Large Array (VLA) images of young SNRs like Tycho (Dickel, van Breugel & Strom, 1991), Kepler (DeLaney et al., 2002), and Cassiopia A (Keohane, Rudnick & Anderson, 1996) show a strong radio emission associated with the shocked ejecta as can be seen in Fig. 2 and 3 (left) for respectively Tycho's and Cassiopia A SNRs. As Rayleigh-Taylor instabilities develop at the interface between the ejecta and the ambient medium, they stretch and compress the magnetic field (Jun & Norman, 1996). This results in an amplified magnetic field in the ambient medium close to the interface, which enhances the synchrotron emission. A thin radio outer filament in front of a weaker plateau is also noticeable around a number of SNRs, presumably

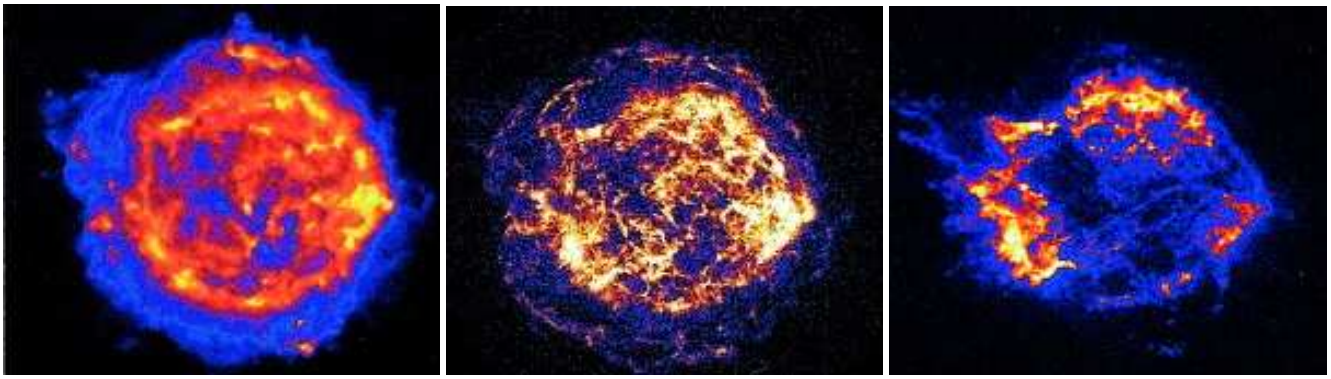

Figure 3: Same caption as Fig. 2, but for the Cassiopia A supernova remnant, see Gotthelf et al. (2001).

associated with the forward shock.

It is only with the advent of *Chandra* and *XMM-Newton* spectro-imagers that the contribution of the shocked ambient medium has been resolved in X-rays from the bright ejecta emission by looking at specific energy bands, like silicon line emission for the ejecta and 4–6 keV continuum for the ambient medium. Figure 2 shows the *Chandra* images of Tycho's SNR, a type Ia supernova, in the continuum and in the silicon line (Hwang et al., 2002). The shocked ambient medium, and in particular the forward shock is visible in the continuum image as a thin filament running at the periphery of the remnant, similar to that seen in radio. The shocked ejecta are best seen in the silicon K emission line. The contact discontinuity, which delineates the extent of the ejecta, is clearly distorted by Rayleigh-Taylor instabilities and lies only slightly inside of the forward shock. As discussed below, in test-particle models, the forward shock (FS) is expected to be well in front of the contact discontinuity (CD). The fact that the forward shock is very close to the contact discontinuity ($R_{\rm FS}/R_{\rm CD} \simeq 1.1$) is a strong morphological argument in favor of efficient particle acceleration at the forward shock. For a type Ia SN (typically n = 7), the expected ratio in the test-particle case is $R_{\rm FS}/R_{\rm CD}$ = 1.18 (Chevalier, 1982), about twice as large as that observed. This also happens to be the case in Kepler's SNR, where the forward shock is very close to the distorted contact discontinuity ($R_{\rm FS}/R_{\rm CD} \simeq 1.1$). An additional example might be SN1006. Long et al. (2003) have proposed that the observed oxygen emission arises from the ejecta. This material is observed to lie close to the outer rims which argues for efficient particle acceleration. The strong observed radio emission (Reynolds & Gilmore, 1986) would then be related to the ejecta, as is proposed for the young SNRs.

Figure 3 shows the *Chandra* images of SNR Cassiopia A in the X-ray continuum and in the silicon line (Gotthelf et al., 2001). The situation is different in this remnant, where except in the northwestern rim the forward shock ($R_{\rm FS}/R_{\rm CD} \simeq 1.25$) is observed to be in front of a weaker X-ray and radio plateau, distant from the distorted contact discontinuity (Gotthelf et al., 2001; Hughes et al., 2000; Hwang et al., 2000). However in Cassiopia A, the hydrodynamical situation is different from the previous cases. Due to its massive progenitor, the ejecta in Cassiopia A are expected to expand in a stellar wind (Chevalier & Oishi, 2003). In such a case, the morphology of the interaction region is modified and in the test-particle case the distance between the forward shock and the contact discontinuity is about twice as large as the same distance in an expansion in a uniform interstellar medium (see Fig. 1). The separation between the contact discontinuity and the forward shock depends also on the index n of the initial ejecta power law profile and varies from $R_{\rm FS}/R_{\rm CD}$ = 1.3 for n = 7 to 1.23 for n = 12. Therefore, in Cassiopia A, it is difficult to draw conclusions about particle efficiency on morphological evidence.

Another distinctive feature of Cassiopia A morphology is its strong and hard X-ray continuum associated with the ejecta, which is not observed in the other remnants considered here (see Fig. 2 and 3). It was first interpreted as synchrotron emission from TeV electrons possibly accelerated at the forward shock (Allen et al., 1997). However, both the fact that the high energy emission (8–15 keV band) is morphologically associated with the interface (Bleeker et al., 2001), and that the estimated magnetic field is very high at this lo-

cation ($B \simeq 1$ mG) are inconsistent with X-ray synchrotron and argue for non-thermal bremsstrahlung at the interface due to particle acceleration at secondary shocks around fast moving knots (Vink & Laming, 2003).

In conclusion, in the remnants of Tycho and Kepler, the position of the forward shock relative to that of the contact discontinuity is consistent with predictions from models of efficient particle acceleration (Chevalier, 1983; Decourchelle et al., 2000).

2.2 Sharp X-ray filaments

In a number of remnants, sharp narrow filaments are observed in radio and recently in X-rays all along the periphery like in Tycho (Hwang et al., 2002), Kepler (Cassam-Chenaï et al., 2004a) and Cassiopia A (Vink & Laming, 2003), in bilateral limbs in SN1006 (Long et al., 2003; Bamba et al., 2003; Rothenflug et al., 2004), or irregularly along the periphery in G347.3−0.5 (Uchiyama, Aharonian & Takahashi, 2003; Lazendic et al., 2004; Cassam-Chenaï et al., 2004b).

The X-ray spectroscopy of these filaments reveals an almost featureless spectrum. If thermal, these spectra would imply a strong ionization delay ($n_e t \simeq 10^8$ s cm^{-3}, Hwang et al., 2000; Cassam-Chenaï et al., 2004a). But the narrow width of the filament is unexpected in thermal models, as they would require a sudden increase of the density just at the position of the forward shock for all of these remnants. If the X-ray spectrum is non-thermal, a synchrotron interpretation is consistent with the fact that the filaments are also observed in radio synchrotron and would imply a maximum energy of accelerated electrons in the range 1–100 TeV. The width of the filaments is then determined by synchrotron losses of ultra-relativistic electrons and allows estimates of the strength of the magnetic field in the filaments (Vink & Laming, 2003). Equating the advection time ($\tau_{\rm ad}$) to the loss time, we obtain an estimation of the downstream magnetic field ($B^{\rm ds}$) as a function of the shock velocity ($V_{\rm s}$), shock compression ratio (R), distance (D), angular size ($\Delta\alpha$) and observed frequency ($\nu_{\rm peak}$) of the filament.

$$B^{\rm ds} = \left(\frac{635}{\tau_{\rm ad}}\right)^{\frac{2}{3}} \left(\frac{1.8\times10^{18}}{\nu_{\rm peak}}\right)^{\frac{1}{3}} \quad (1)$$

Table 1:

SNR	D(kpc)	$V_{\rm s}$(km s^{-1})	$\Delta\alpha$	$B^{\rm ds}_{\rm tp}(\mu$G)
Tycho	2.3	4600	$\leq 4''$	$\simeq 75$
Kepler	4.8	5400	$\leq 3''$	$\simeq 60$
Cas A	3.4	5400	$\leq 4''$	60–100

$$\tau_{\rm ad} = \frac{R\,\Delta\alpha\,D}{V_{\rm s}} \quad (2)$$

Table 1 sums up SNR parameters and estimates of the downstream magnetic field in three SNRs assuming a compression ratio of four. In this case, the derived values of the magnetic field are inconsistent with a simple test-particle compression of the standard interstellar magnetic field ($\simeq 3$ μG) at the shock and require that the magnetic field has been further amplified as theoretically proposed by Lucek & Bell (2000). On the other hand, if efficient acceleration occurs (as suggested in the previous section), compression ratios $R_{\rm nl}$ larger than four are expected as shown in Fig. 1. The estimated downstream and upstream magnetic fields are then much smaller than in the test-particle case and for a perpendicular magnetic field, we have:

$$B^{\rm ds}_{\rm nl} = \left(\frac{4}{R_{\rm nl}}\right)^{2/3} B^{\rm ds}_{\rm tp} \quad (3)$$

$$B^{\rm ups}_{\rm nl} = \frac{B^{\rm ds}_{\rm tp}}{R_{\rm nl}} = \frac{4^{2/3}}{R_{\rm nl}^{5/3}}\, B^{\rm ds}_{\rm tp} \quad (4)$$

For a compression ratio $R_{\rm nl}$ of 10, the derived upstream magnetic field ($\simeq$ 3–5 μG) is then roughly consistent with the interstellar magnetic field value. However, the intrinsic width of the filament is expected to be even smaller than the observed projected angular size $\Delta\alpha$, and thus the previous estimates give only lower limits on the downstream magnetic field in the filaments. If the intrinsic width of the observed filaments is significantly smaller than observed, further magnetic amplification will be required as well.

The high values of the downstream magnetic field at the forward shock are of crucial importance for the acceleration of cosmic rays at energies close to the knee. Indeed, it shows that the observed electron spectrum is limited at high energy by synchrotron losses and allows the maximum energy of accelerated ions to be much larger than that of the electrons.

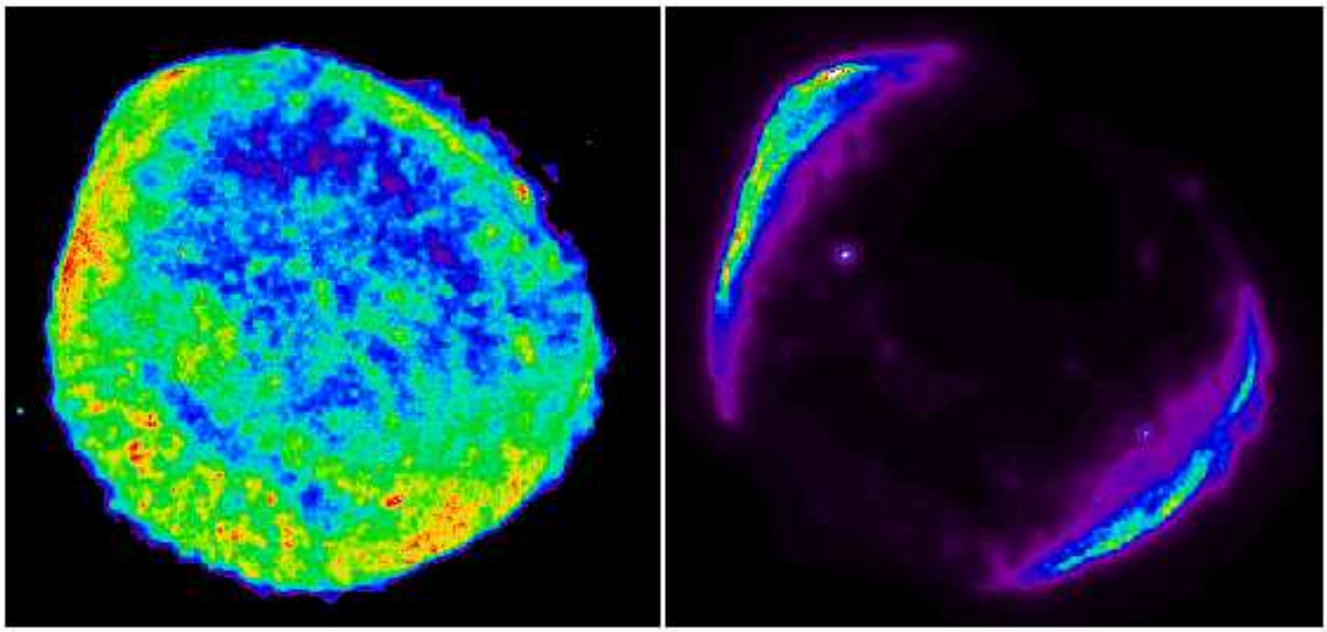

Figure 4: *XMM-Newton* X-ray images of the SN1006 supernova remnant. Left: in the oxygen K-line band (0.5–0.8 keV). Right: in the high energy 2–4.5 keV band, where the non-thermal emission dominates. From Rothenflug et al. (2004).

3 Particle acceleration at the reverse shock?

While there are indications that the forward shock in SNRs is an efficient particle accelerator, the status of the reverse shock is far less clear (Ellison et al., 2005). Like the forward shock, it is a high Mach-number shock. However, because of the rapid adiabatic expansion of the ejecta, the initial magnetic field of the progenitor is vastly diluted and the reverse shock is not expected to produce relativistic particles, except in the extreme case of a white dwarf progenitor with a huge magnetic field ($B \simeq 10^{10}$ G).

Observing radio (or X-ray) synchrotron emission at the reverse shock has thus strong implications for the strength of the magnetic field in the unshocked ejecta, requiring important amplification of the initial progenitor magnetic field. There are a few supernova remnants, where a possible synchrotron emission of the reverse shock has been proposed. In Cassiopia A, the coinciding rapid drop of both the radio and X-ray silicon line brightness has been interpreted in terms of the position of the reverse shock (Gotthelf et al., 2001) and would imply that shocked ejecta emit radio synchrotron emission. In RCW86, the soft X-ray morphology is well correlated with that of the Hα emission, lying along the outer boundary of the remnant, while the hard X-ray emission is observed toward the interior, close to the radio emission (Rho et al., 2002). The hard emission, interpreted as synchrotron, is associated with the iron 6.4 keV emission, presumably originating from the ejecta. This would argue for synchrotron X-rays from the ejecta. Finally in Kepler's SNR, VLA radio observations at 6 and 20 cm have been used to derive the variations of the spectral index over the remnant (DeLaney et al., 2002). While regions with flat spectral index are associated with the forward shock, regions of steep spectral index have been proposed to be associated with the ejecta.

On the other hand, if the reverse shock does accelerate efficiently particles to relativistic energies, the morphology of the shocked ejecta will be modified, which strongly impacts the X-ray emission. The temperature of the shocked ejecta will get much lower than in the test-particle case – too low to produce the iron K line at about 6.5 keV observed in Kepler, Tycho and Cassiopia A (Decourchelle et al., 2000). Therefore, inefficient acceleration at the reverse shock is probably required in most young SNRs.

4 Synchrotron-dominated SNRs

We have previously examined the different possible observational constraints on particle acceleration in young ejecta-dominated supernova remnants. In this section, we will focus on two supernova remnants, whose X-ray emission is dominated by non-thermal

emission. SN1006 was the first case where limb-brightened non-thermal emission was discovered in a shell-like supernova remnant using the *ASCA* satellite (Koyama et al., 1995). The *ASCA* satellite revealed two other shell-like remnants dominated by non-thermal emission: G347.3−0.5 (Koyama et al., 1997; Slane et al., 1999) and G266.2−1.2 (Slane et al., 2001). In the following, we will present the latest observational results for SN1006 and G347.3−0.5 obtained with *XMM-Newton* and *Chandra*. These new observations allow us to image and characterize the synchrotron emission over these remnants. The use of radio data provides strong constraints by anchoring the low energy part of the energy electron spectrum.

4.1 Geometry of the acceleration in SN1006

A full coverage of the SN1006 remnant (angular size of about $30'$) has been carried out with the *XMM-Newton* satellite thanks to its large field of view and unprecedented sensitivity. Figure 4 shows the thermal and non-thermal morphology of SN1006 (Rothenflug et al., 2004). The thermal contribution is best mapped in the oxygen band (0.5–0.8 keV) and shows diffuse extended emission. In contrast, the non-thermal emission dominant at higher energies (2–4.5 keV) has a relatively sharp bipolar morphology with bright north-eastern and southwestern rims. An apparent symmetry axis in the radio and high energy X-ray data is running from south-east to north-west. Initially this symmetry was proposed to represent the direction of the magnetic field (Reynolds, 1996). The compressed tangential component of the magnetic field is then larger at the northeastern and southwestern rims and naturally explains the enhanced synchrotron emission in the rims. However, in such a magnetic configuration, not only these limbs, but the complete equatorial belt is expected to have larger compressed magnetic field and non-thermal emission should also be seen in projection in the interior. The new observations can set an upper limit on the emission from the center. The brightness profile transverse to the limbs in the 2–4.5 keV band shows a very steep decrease toward the interior, which is incompatible with an equatorial belt, and strongly suggests that the bright non-thermal limbs are polar caps (Rothenflug et al., 2004). Such a configuration is favored by particle acceleration model as the particle injection is larger for parallel shocks (Völk et al., 2003). However, it raises the problem that if polar caps are a common configuration, we should observe non-thermal synchrotron center-filled remnant, which is not the case (Fulbright & Reynolds, 1990).

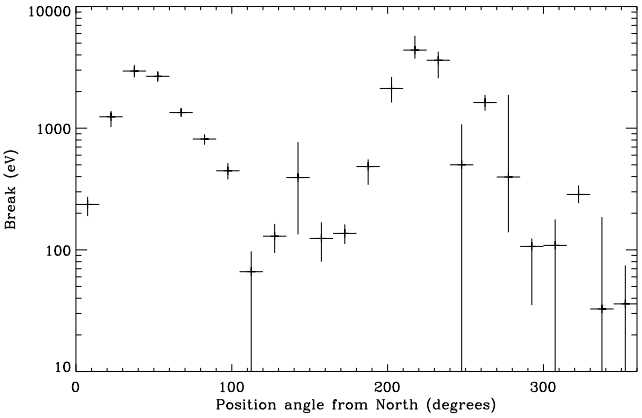

Figure 5: Azimuthal variation close to the shock of the cut-off frequency of the synchrotron component in SN1006. The two peaks correspond to the bright limbs: northeastern limb on the left and southwestern rim on the right, see Rothenflug et al. (2004).

Radio and X-ray data can be used simultaneously to constrain the synchrotron spectrum in supernova remnants. Using *ASCA* data, this approach has been taken to characterize the non-thermal spectrum of SN1006, globally (Dyer et al., 2001) and in specific regions such as the limbs, center, and caps (Dyer et al., 2004). Recently, Rothenflug et al. (2004) obtained the radial and azimuthal variations of the synchrotron emission in SN1006. Using combined VLA and Parkes data at 1517 MHz (FWHM: $23'' \times 13''$) and *XMM-Newton* data, Rothenflug et al. (2004) have fitted the observed photon spectrum with a synchrotron model from a cut-off electron power law (SRCUT in `XSPEC`, Reynolds, 1998)) and a thermal non equilibrium ionization model. The normalization and spectral index of the synchrotron component are fixed by radio data and only the cut-off frequency is allowed to vary. Figure 5 shows the very strong azimuthal variations of the cut-off frequency, which cannot be explained by variations of the magnetic compression alone. The maximum energy of accelerated particles is higher at the bright limbs than elsewhere. For a magnetic field of about 50 μG, the maximum energy reached by the electrons at the bright northeastern limb is around 100 TeV.

In conclusion, the X-ray geometry of SN1006 favors cosmic ray acceleration where the magnetic field was originally parallel to the shock speed, i.e., a polar cap configuration.

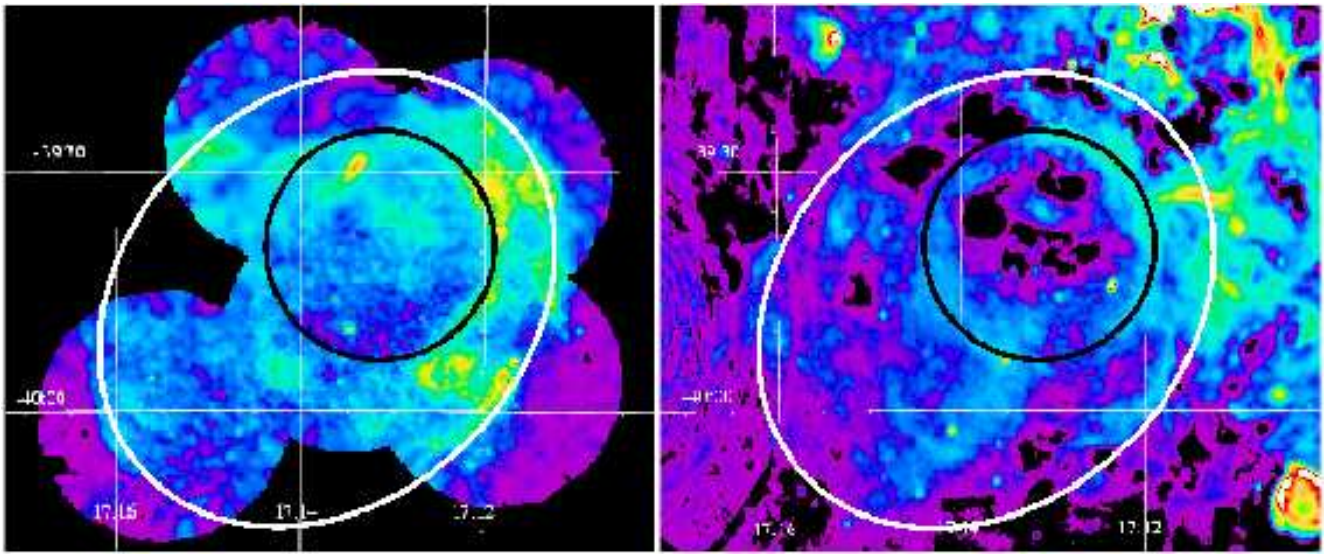

Figure 6: G347.3−0.5 supernova remnant. Left: *XMM-Newton* X-ray mosaic in the 2–10 keV band (Cassam-Chenaï et al., 2004b). Right: ATCA radio image at 1.4 GHz (Lazendic et al., 2004).

4.2 An extreme case: G347.3−0.5

The second synchrotron dominated shell-like supernova remnant, G347.3−0.5, differs from SN1006 in many points. First, instead of the regular bipolar morphology of the type Ia SN1006, G347.3−0.5 has an irregular and distorted morphology as shown in Fig. 6. Proposed to be located at 6 kpc, close to the Galactic plane, the remnant is thought to be interacting with nearby molecular clouds (Slane et al., 1999) and is associated with γ-ray GeV and TeV (Muraishi et al., 2000) emission, whose nature is still debated (Butt et al., 2002; Enomoto et al., 2002; Reimer & Pohl, 2002).

A second difference, which makes G347.3−0.5 more extreme, is that in any place the X-ray spectrum is entirely dominated by non-thermal emission and no thermal emission has been detected (Slane et al., 1999; Pannuti et al., 2003; Lazendic et al., 2004; Cassam-Chenaï et al., 2004b). In the radio regime, the synchrotron emission is very faint and irregular (see Fig. 6 right), and lies in a crowded region close to the Galactic plane (Lazendic et al., 2004). *Chandra* observations have been carried out on specific bright fields (Uchiyama, Aharonian & Takahashi, 2003; Lazendic et al., 2004). As shown in Fig. 6 (left), the large extent of the remnant (about $70' \times 50'$) has been almost covered by five pointings with *XMM-Newton* (Cassam-Chenaï et al., 2004b). Due to the faint radio emission of the SNR and contaminated field, it has not been possible to use the radio data to constrain the synchrotron spectrum as was done for SN1006. The synchrotron emission was thus characterized over the remnant only in the X-ray band using an absorbed power-law model.

Strong variations of the interstellar absorption (from 4×10^{21} to 1×10^{22} cm^{-2}) are observed over the remnant. The highest absorption is found in the southwestern and northwestern rims, where the X-ray brightness is the largest, while the center and southwestern rim have the lowest absorption and fainter X-ray emission. This behavior is in contradiction with what we would expect from increasing intervening material in the line of sight: the higher the absorption, the lower the emission particularly at low energy. The clear positive correlation between brightness and absorbing column density, shown in Fig. 7, argues for an interaction between dense material and the SNR in the brightest regions. This interaction enhances the non-thermal emission. Depending on the distance of the supernova remnant (6 kpc or 1 kpc), the density of the interstellar material is estimated to lie between 50 and 300 part cm^{-3}.

The comparison, in different lines of sight toward the remnant, of the X-ray derived absorption and integrated H I and CO radio profile as a function of the velocity has forced to revise the distance of G347.3−0.5. The fact that the absorption is larger in the southwest than in the northwest is incompatible with a large dis-

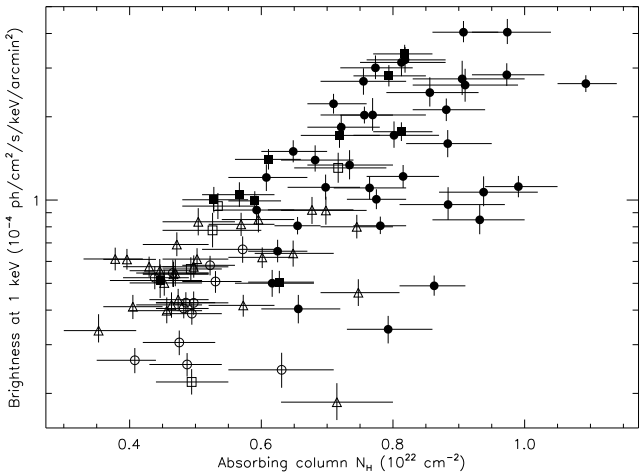

Figure 7: G347.3−0.5: correlation plot between the normalized synchrotron brightness at 1 keV and the absorbing column density (in units of 10^{22} cm^{-2}). The error bars are given at a 90% confidence level.

tance of 6 kpc. Above a distance of 3 kpc the integrated H I and CO density is much larger in the northwest than in the southwest. Recent CO observations have revealed the presence of CO clouds at about 1 kpc, whose distribution is well correlated with the brightest regions of the SNR (Fukui et al., 2003).

The characterization of the synchrotron emission over the remnant has revealed large variations of the spectral index from place to place (from α = 1.8 to 2.6). The spectrum is the flattest in the southeastern rim, where the emission is faint and is steeper in the brightest regions. This is a situation inverse to that of SN1006, in which the bright limbs exhibit the hardest spectrum. In the interior, the spectrum is also steep as expected from the softening due to synchrotron losses. The physics of particle acceleration in G347.3−0.5 is clearly driven by the interaction of the remnant with ambient molecular clouds unlike SN1006, which is evolving in a relatively uniform low density interstellar medium. A better characterization of the properties of the synchrotron emission in places where the remnant is interacting with clouds needs to be done to confront theoretical predictions (Bykov et al., 2000).

5 Conclusions

In this review, we have shown the great potential of combining radio and X-ray data to investigate particle acceleration in supernova remnants. Synchrotron radio data provide information on the bulk of the relativistic electron population while X-ray synchrotron emission reveals the high energy end of the electron distribution. We have shown that morphological arguments are powerful to estimate the level of efficiency of particle acceleration, as well as the magnetic field strength and orientation. While X-ray thermal emission is essential to determine the evolutionary stage of the remnant, radio thermal emission (H I, CO) are required to investigate the interstellar environment in which the remnant is evolving.

Acknowledgments

I wish to warmly thank my colleagues Jean Ballet, Gamil Cassam-Chenaï, Gloria Dubner, Don Ellison, Elsa Giaccani, Jack Hughes, Una Hwang and Rob Petre for fruitful discussions and collaborations. I thank the organizers for a very constructive meeting.

References

Allen, G. E., et al. 1997, ApJ, 487, L97

Bamba, A., Yamazaki, R., Ueno, M., Koyama, K. 2003, ApJ, 589, 827

Berezhko, E. G., Ellison, D. C. 1999, ApJ, 526, 385

Bleeker, J. A. M., Willingale, R., van der Heyden, K., Dennerl, K., Kaastra, J. S., Aschenbach, B., Vink, J. 2001, A&A, 365, L225

Blondin, J. M., Ellison, D. C. 2001, ApJ, 560, 244

Butt, Y. M., Torres, D. F., Romero, G. E., Dame, T. M., Combi, J. A. 2002, Nature, 418, 499

Bykov A. M., Chevalier, R. A., Ellison, D. C., Uvarov, Y. A. 2000, ApJ, 538, 203

Cassam-Chenaï, G., Decourchelle, A., Ballet, J., Hwang, U., Hughes, J. P., Petre, R. 2004a, A&A, 414, 545

Cassam-Chenaï, G., Decourchelle, A., Ballet, J., Sauvageot, J. L., Dubner, G., Giaccani, E. 2004b, A&A, 427, 199

Chevalier, R. A. 1982, ApJ, 258, 790

Chevalier, R. A. 1983, ApJ, 272, 765

Chevalier, R. A., Blondin, J. M. 1995, ApJ, 444, 312

Chevalier, R. A., Oishi, J. 2003, ApJ, 593, L23

Decourchelle, A., Ellison, D., Ballet, J. 2000, ApJ, 543, L57

Decourchelle, A., Sauvageot, J. L., Audard, M., Aschenbach, B., Sembay, S., Rothenflug, R., Ballet, J., Stadlbauer, T., West, R. G. 2001, A&A, 365, L218

DeLaney, T., Koralesky, B., Rudnick, L., Dickel, J. R. 2002, ApJ, 580, 914

Dickel, J. R., van Breugel, W. J. M., Strom, R. G. 1991, AJ, 101, 2151

Drury, L. O'C. 1983, Rep. Prog. Phys., 46, 973
Drury, L. O'C., et al. 2001, SSRv, 99, 329
Dyer, K. K., Reynolds, S. P., Borkowski, K. J. 2004, ApJ, 600, 752
Dyer, K. K., Reynolds, S. P., Borkowski, K. J., Allen, G. E., Petre, R. 2001, ApJ, 551, 439
Ellison, D., Decourchelle, A., Ballet, J. 2004, A&A, 413, 189
Ellison, D., Decourchelle, A., Ballet, J. 2005, A&A, 429, 569
Enomoto, R., et al. 2002, Nature, 416, 823
Fukui, Y., et al. 2003, PASJ, 55, L61
Fulbright, M. S., Reynolds, S. P. 1990, ApJ, 357, 591
Gotthelf, E. V., Koralesky, B., Rudnick, L., Jones, T. W., Hwang, U., Petre, R. 2001, ApJ, 552, L39
Hughes, J. P., Rakowski, C. E., Burrows, D. N., Slane, P. O. 2000, ApJ, 528, L109
Hwang, U., Decourchelle, A., Holt, S. S., Petre, R. 2002, ApJ, 581, 1101
Hwang, U., Holt, S. S., Petre, R., 2000, ApJ, 537, L119
Jun, B.-I., Norman, M. L. 1996, ApJ, 472, 245
Jun, B.-I., Jones, T. W., Norman, M. L. 1996, ApJ, 468, L59
Keohane, J. W., Rudnick, L., Anderson, M. C. 1996, ApJ, 466, 309
Kirk, J. G. 2005, these proceedings
Koyama, K., Kinugasa, K., Matsuzaki, K., Nishiuchi, M., Sugizaki, M., Torii, K.,Yamauchi, S., Aschenbach, B. 1997, PASJ, 49, L7
Koyama, K., Petre, R., Gotthelf, E. V., Hwang, U., Matsuura, M., Ozaki, M., Holt, S. S. 1995, Nature, 378, 255
Lazendic, J. S., Slane, P. O., Gaensler, B. M., Reynolds, S. P., Plucinsky, P. P., Hughes, J. P. 2004, ApJ, 602, 271
Long, K. S., Reynolds, S. P., Raymond, J. C., Winkler, P. F., Dyer, K. K., Petre, R. 2003, ApJ, 586, 1162
Lucek, S. G., Bell, A. R. 2000, MNRAS, 314, 65
Muraishi, H., et al. 2000, A&A, 354, L57
Pannuti, T. G., Allen, G. E., Houck, J. C., Sturner, S. J. 2003, ApJ, 593, 377
Reimer, O., Pohl, M. 2002, A&A, 390, L43
Reynolds, S. P. 1996, ApJ, 459, L13
Reynolds, S. P. 1998, ApJ, 493, 375
Reynolds, S. P. 2005, these proceedings
Reynolds, S. P., Gilmore, D. M. 1986, AJ, 92, 1138
Rho, J., Dyer, K. K., Borkowski, K. J., Reynolds, S. P. 2002, ApJ, 581, 1116
Rothenflug, R., Ballet, J., Dubner, G., Giaccani, E., Decourchelle, A., Ferrando, P. 2004, A&A, 425, 121
Slane, P., Gaensler, B. M., Dame, T. M., Hughes, J. P., Plucinsky, P. P., Green, A. 1999, ApJ, 525, 357
Slane, P., Hughes, J. P., Edgar, R. J., Plucinsky, P. P., Miyata, E., Tsunemi, H., Aschenbach, B. 2001, ApJ, 548, 814
Tanimori, T., et al. 1998, ApJ, 497, L25
Uchiyama, Y., Aharonian, F. A., Takahashi, T. 2003, A&A, 400, 567
Vink, J., Laming, J. M. 2003, ApJ, 584,758
Völk, H. J., Berezhko, E. G., Ksenofontov, L. T. 2003, A&A 409, 563